CRYSTAL GROWTH & DESIGN

Article

Cite This: Cryst. Growth Des. 2018, 18, 5301−5310

pubs.acs.org/crystal

Chloride Flux Growth of Idiomorphic AWO_4 (A = Sr, Ba) Single Microcrystals

Kenta Kawashima,[†,◆] Jun-Hyuk Kim,[‡,◆] Isabelle Cheng,[‡] Kunio Yubuta,[§] Kihyun Shin,[†,∥] Yang Liu,[‡,⊥] Jie Lin,[‡,#] Graeme Henkelman,[†,∥] and C. Buddie Mullins*[,†,‡,▽]

[†]Department of Chemistry, [‡]John J. McKetta Department of Chemical Engineering, [∥]Institute for Computational Engineering and Sciences, and [▽]Texas Materials Institute, The University of Texas at Austin, Austin, Texas 78712, United States

[§]Institute for Materials Research, Tohoku University, 2-1-1 Katahira, Aoba-ku, Sendai 980-8577, Japan

[⊥]College of Chemistry and Chemical Engineering, Central South University, Changsha, Hunan 410083, China

[#]Pen-Tung Sah Micro-Nano Science and Technology Institute, Xiamen University, Xiamen, Fujian 361005, China

Supporting Information

ABSTRACT: Scheelite-type divalent metal tungstate materials (AWO_4) have been studied for various applications due to their attractive mechanical and chemical properties. Preparation of the shape-controlled AWO_4 crystals with high crystallinity is one of the most effective approaches for further exploring and improving their properties. In this study, highly crystalline $SrWO_4$ and $BaWO_4$ microcrystals with different morphologies were grown by using a chloride flux growth technique. To investigate the effect of growth conditions on $SrWO_4$ and $BaWO_4$ crystals, NaCl and KCl were used as a flux, and the solute concentration was adjusted in the range of 5−50 mol %. The difference in the flux cation species (Na^+ and K^+) mainly affected the crystal size. In accordance with increasing the solute concentration, the dominant crystal shape of $SrWO_4$ and $BaWO_4$ varied as follows: whisker (a rod- or wire-like morphology with a large aspect ratio) → platelet → well/less-faceted polyhedron. Additionally, according to scanning electron microscopy and transmission electron microscopy results, a dendritic morphological transformation from AWO_4 whisker to platelet during crystal growth has been proposed.

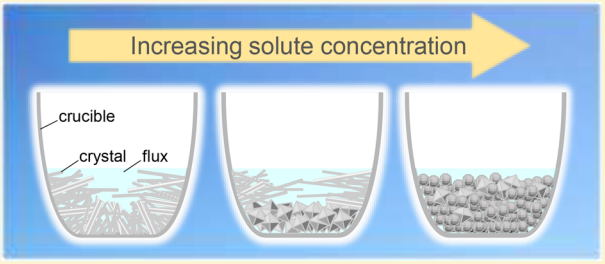

INTRODUCTION

Recently, divalent metal tungstate materials have attracted attention because of their promising applications in mobile telecommunications,[1] photoluminescence,[2] optical fibers,[3] inorganic scintillating materials,[4] sensors,[5] photocatalysis,[6] and electrocatalysis.[7] Among them, tetragonal $BaWO_4$ and $SrWO_4$ (scheelite-type structure: tetrahedrons consisting of four corner O^{2-} ions and a central W^{6+} ion are separated from each other, while Ba^{2+} and Sr^{2+} ions are surrounded by eight O^{2-} ions)[8] are typical materials with the space group $I4_1/a$ (Figure S1, the crystal structures were drawn with VESTA version 3.3.2).[9−11] Since $BaWO_4$ and $SrWO_4$ have attractive mechanical and chemical properties as well as dielectric properties, ε_γ = 8.4 and 8.6; $Q \times f$ = 58 800 and 57 500 GHz; and τ_f = −64 and −52 ppm·°C^{-1}, respectively,[12] they have been extensively studied.

In order to further explore and improve their properties, morphological control techniques have been studied as a critical approach. For instance, Sczancoski et al. reported the growth of pitch and longleaf pine cone-like $SrWO_4$ microcrystals using different strontium precursors,[13] Sahmi et al. grew porous $CaWO_4$ and $SrWO_4$ thin films via spray pyrolysis,[14] Cheng et al. introduced high energy ball milling methods (mechanochemical method) to prepare AWO_4 (A = Ca, Ba, Sr) nanopowders,[12] and Li et al. synthesized $SrWO_4$ micro-octahedrons, shuttles, pillars, and flowers by using an electrochemical-assisted precipitation method.[15] In addition to exploring the morphological control techniques, investigations for obtaining highly crystalline products might also be beneficial for further studies regarding their crystal anisotropy and isotropy, which can change the mechanical properties and chemical and physical adsorption (i.e., chemisorption and physisorption) behavior of $BaWO_4$ and $SrWO_4$.

A flux method (a molten-salt method) is a type of liquid-phase growth method and one of the most simple and versatile methods for single crystal growth.[16−18] Introducing flux for inorganic crystal growth is very effective for obtaining crystals having highly crystalline, preferentially grown facets, and a low impurity concentration along with a low growth temperature (600−1300 °C).[16] There are a lot of reports about the advantages of flux: controlling thermal stress,[18] minimizing crystal defects,[19] deforming crystal shape,[20] developing crystal facets,[21] and so on. Moreover, it has been reported that $Ba_2Mg(B_3O_6)_2$ (BMBO), $Y_3Fe_5O_{12}$ (YIG), and

Received: May 16, 2018
Revised: July 23, 2018
Published: July 24, 2018

DOI: 10.1021/acs.cgd.8b00757
Cryst. Growth Des. 2018, 18, 5301−5310

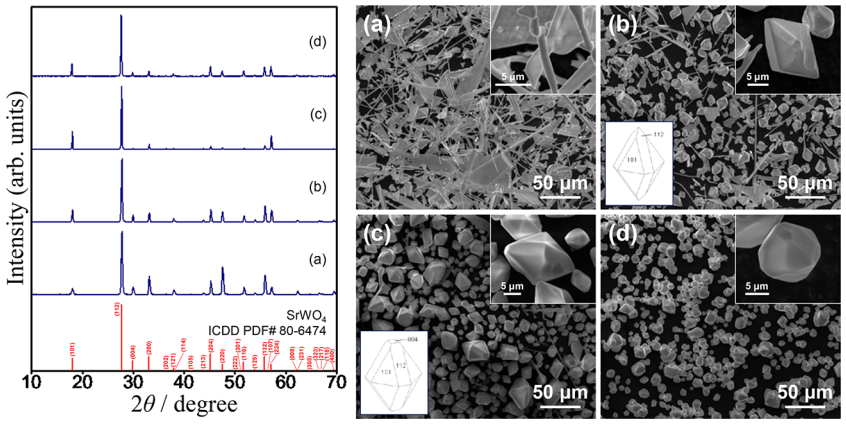

Figure 1. XRD patterns and SEM images of the $SrWO_4$ crystals grown using the NaCl flux with solute concentrations: (a) 5, (b) 10, (c) 20, and (d) 50 mol %.

$Be_3Al_2Si_6O_{18}$:Cr (emerald) crystals, which are incongruent-melting materials at high temperature, were successfully grown by the flux method at comparatively low temperature as stable structures.[22−24] Previously, choosing suitable fluxes for certain materials was quite difficult, and the fluxes were chosen via a trial and error approach based on previous experience. Fortunately, since a guide to the choice of suitable fluxes for oxide crystal growth was systematically constructed taking into account the material fundamental parameters (e.g., ionic radius, melting point, chemical bonding iconicity, Dietzel's parameter, and acidity and basicity) by Oishi et al.,[25] we can now easily select the desired fluxes for certain oxide crystal growths. The useful aspects of flux methods have been well documented, and there are several reports suggesting the impact of fluxes (e.g., LiCl, NaCl, KCl, CsCl, LiCl−NaCl, NaCl−KCl−CsCl, $BaCl_2$, $LiNO_3$, and $Na_2W_2O_7$) on the $SrWO_4$ and $BaWO_4$ crystal growth (i.e., lowering the synthesis temperature, developing their crystal facets, growing high-quality single crystals, etc.).[26−37] In most of those reports, however, the shapes of the grown crystals were not optimal. Even though other crystal shapes such as needles, plates, and other nonuniform shapes were also reported,[28,32,33,35] these results provide largely fragmentary information, which is also somewhat controversial, especially regarding crystal-morphological formation mechanisms.

In this study, we report the sodium- and potassium-chloride flux growth of scheelite-type $SrWO_4$ and $BaWO_4$ crystals with unique morphologies and high crystallinity. Sodium chloride and potassium chloride are expected to be an excellent flux because of their relatively high solubility in water, which allow us to segregate the as-grown crystals from the remaining fluxes easily.[38] Additionally, the cationic valencies (+1) of NaCl and KCl fluxes are different from those (+2) of $SrWO_4$ and $BaWO_4$ (solute), which might prevent the solid solution formation between the flux and the solute.[39] Here, the flux and solute concentration effect on resultant $SrWO_4$ and $BaWO_4$ crystals were investigated in detail. This study attempts to reveal both their crystal-morphological and phase formation mechanisms.

EXPERIMENTAL SECTION

Growth of $BaWO_4$ and $SrWO_4$ Crystals. Scheelite-type $BaWO_4$ and $SrWO_4$ crystals were synthesized by a chloride flux method. $BaCO_3$ (99.7%, Fisher Scientific Co.), $SrCO_3$ (≥99.9%, Aldrich Chemical Co.), and WO_3 (99.8%, Alfa Aesar Co.) were mixed together with an adjusted amount of NaCl (≥99.0%, Fisher Scientific Co.) or KCl (99.5%, Fisher Scientific Co.) by manually grinding with an alumina mortar and pestle. Here, the solute concentration was adjusted from 5 to 50 mol %. The as-prepared powder mixtures were placed into an alumina crucible, heated at a rate of 150 °C·h^{-1} to 900 °C for 10 h in an electrical muffle furnace, and then cooled naturally to room temperature followed by rinsing with water to remove the remaining flux. To study the phase transformation and flux effect on the morphology of $BaWO_4$ and $SrWO_4$ crystals, they were also prepared using solid-state reaction techniques with a heating rate of 150 °C·h^{-1}, holding temperatures of 300, 600, and 900 °C, and holding times of 0 and 10 h.

Characterization. All the as-grown crystals (without grinding) were structurally characterized by X-ray diffraction (XRD, Mini-Flex600, Rigaku) equipped with Cu Kα radiation in the 2θ scan range of 10−70°. The crystal morphology was observed using environmental scanning electron microscopy (ESEM, Quanta 650, FEI). A drawing of typical as-grown crystals was obtained using QuartzVS version 5.02. The crystallographic characteristics of the as-grown crystals were analyzed by high-resolution transmission electron microscopy (HR-TEM, EM-002B, TOPCON) operated at 200 kV.

Computational Details. Plain-wave-based spin-polarized density functional theory (DFT) calculations were performed with the Vienna ab initio simulation package (VASP).[40−42] Core electrons were described within the projector augmented-wave (PAW) framework,[43] and the electronic exchange and correlation energies were described within the generalized gradient approximation using the revised Perdew−Burke−Ernzerhof (RPBE) functional.[44,45] Valence electron functions were expanded in a plane-wave basis up to a cutoff energy of 400 eV. We employed a Gaussian smearing with a width of 0.05 eV to improve the convergence near the Fermi level. The Brillouin zone was sampled with a 2 × 2 × 1 Monkhost-Pack k-point mesh. The convergence criteria for electronic structure and geometry were set to 10^{-5} eV and 0.01 eV·Å^{-1}, respectively. We prepared AWO_4 (A = Sr, Ba) slab systems having (100), (010), (001), and (110) surfaces. Each slab contained four layers with the bottom two layers fixed in their bulk position.

RESULTS AND DISCUSSION

Effect of Flux and Solute Concentration on Growth of $SrWO_4$ Crystals. To investigate the effect of flux (NaCl and KCl) and solute concentration (5−50 mol %) on the growth of $SrWO_4$ crystals, the resultant phase and morphology of the as-grown crystals were identified and observed with XRD and scanning electron microscopy (SEM) measurements, respectively. The XRD patterns of the crystals grown using the NaCl flux with different solute concentrations ranging from 5 to 50 mol % are shown in Figure 1. All the diffraction patterns were attributable to tetragonal $SrWO_4$ (ICDD PDF# 80-6474)

DOI: 10.1021/acs.cgd.8b00757
Cryst. Growth Des. 2018, 18, 5301−5310

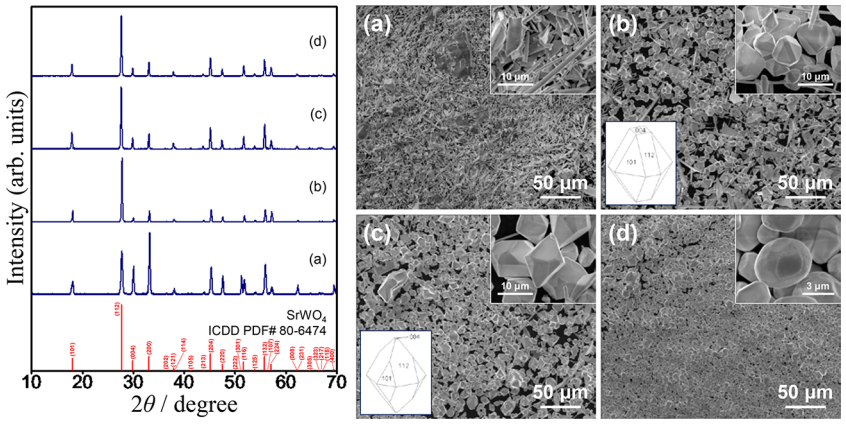

Figure 2. XRD patterns and SEM images of the $SrWO_4$ crystals grown using the KCl flux with solute concentrations: (a) 5, (b) 10, (c) 20, and (d) 50 mol %.

without any diffraction peaks corresponding to impurity phases such as Na^+ and/or Cl^- driven phases, indicating that the NaCl flux led to no impurity growth. At the solute concentrations of 5 and 10 mol %, the (004)/(112), (200)/(112), and (220)/(112) peak intensity ratios (5 mol %: 0.13, 0.30, 0.50; 10 mol %: 0.09, 0.15, 0.17) were higher than those at the solute concentrations of 20 and 50 mol % (20 mol %: 0.02, 0.08, 0.02; 50 mol %: 0.07, 0.09, 0.09), implying that the $SrWO_4$ crystals grown using the NaCl flux with lower solute concentrations were relatively abundant in {001}, {100}, and {110} facets. Interestingly, a clear difference in crystal morphology can be found among the four samples as shown in the SEM images (Figure 1), indicating that the $SrWO_4$ crystals grown using the NaCl flux were significantly affected by the solute concentration. At the lowest solute concentration (5 mol %), the as-grown $SrWO_4$ crystals showed mainly whisker-shaped morphology as well as plate-shaped and granular-shaped (ca. 28 μm) morphologies. As the solute concentration was increased, both the whisker- and plate-shaped particles were less prevalent, while the granular particles became more prevalent. At a solute concentration of 10 mol %, the as-grown $SrWO_4$ crystal products became a mix of small irregular hexadecagonal crystals (ca. 18 μm) bounded by {112} and {101} facets, plate-shaped crystals, and whisker-shaped crystals. At a solute concentration of 20 mol %, the as-grown $SrWO_4$ particles had an approximate size of 20 μm and were an irregular octadecagonal shape bounded by {112}, {101}, and {001} facets, and at a solute concentration of 50 mol %, the as-grown $SrWO_4$ particles became rounder (i.e., a polyhedronal shape) with a diameter of around 7.6 μm.

Figure 2 shows the XRD patterns of the crystal products grown using KCl flux with different solute concentrations (5–50 mol %). All the diffraction patterns were identified as a tetragonal $SrWO_4$ phase without any impurity phases. It is worth noting that, at a solute concentration of 5 mol %, the as-grown crystals have the higher (004)/(112) and (200)/(112) peak intensity ratios of 0.42 and 1.04 as compared to the reference sample with the intensity ratios of 0.16 (004)/(112) and 0.22 (200)/(112) due to the abundance of {001} and {100} facets on our $SrWO_4$ crystals grown using KCl flux with the lowest solute concentration. SEM images of the $SrWO_4$ crystals grown using the KCl flux with different solute concentrations are shown in Figure 2. Here, the solute concentration greatly influenced the resultant crystal morphologies again. At a solute concentration of 5 mol %, the as-grown $SrWO_4$ crystals predominantly had both whisker- and plate-like shapes, and a relatively small amount of granular-shaped crystals (ca. 14 μm) were also observed. At a solute concentration of 10 mol %, the dominant $SrWO_4$ crystal shape was an irregular octadecagon (ca. 8.3 μm) rather than whisker or platelet. At a solute concentration of 20 mol %, the $SrWO_4$ octadecagons with an approximate size of 7.9 μm were mainly formed. As shown in Figure 2b,c, the $SrWO_4$ octadecagons formed at the solute concentrations of 10 and 20 mol % were bounded by well-developed {112}, {101}, and {001} facets. The $SrWO_4$ particles grown with a solute concentration of 50 mol % possessed irregular polyhedral shapes (3–20 μm diameter).

Dendritic crystals were found for any conditions in which whiskers were generated: some whiskers have branches that appeared along one or two sides of the whisker. In both the NaCl and KCl flux growth cases, the crystals grown with lower solute concentrations tend to form idiomorphic shapes with clear edges because of the higher solute solubility, allowing the $SrWO_4$ crystals to grow freely and gain their idiomorphic shapes in the supersaturated molten salt solutions. With increasing solute concentration, the crystal shape transition (whisker/dendrite → platelet → hexadecagon/octadecagon → polyhedron) was observed with either NaCl or KCl, suggesting that the cationic species (Na^+ and K^+) in chloride fluxes do not have a great effect on the resultant crystal morphology. Remarkably, although the NaCl and KCl flux-grown crystals had the same trend in the crystal shape transition, all the sizes of the NaCl flux-grown crystals were slightly larger than those of the KCl flux-grown crystals probably due to the difference in the solubility of the solute in the flux. It is reported that the solubility is high if the difference between the cation sizes of the two components (solute and flux) is high.[46] Accordingly, the solubility of $SrWO_4$ in NaCl might be higher compared to that in KCl, judging from the ionic radii of Na^+ (r_{ionic} = 1.02 Å: CN = 6), K^+ (r_{ionic} = 1.38 Å: CN = 6), and Sr^{2+} (r_{ionic} = 1.26 Å: CN = 8),[47] and this high NaCl-solubility induces the smaller crystals to be more soluble in a flux and crystallize on the larger crystals to minimize the specific surface free-energy during the crystal growth, resulting in larger $SrWO_4$ crystals of any shapes, which can be expressed as flux-assisted Ostwald ripening.[48−50] Furthermore, according to a previous report and our result (for details about the method to measure the solubility, see Supporting Information and Figure S2),[28] the solubilities of $SrWO_4$ in NaCl and KCl at 900 °C are 4.8 mol % (29 g/100 g

DOI: 10.1021/acs.cgd.8b00757
Cryst. Growth Des. 2018, 18, 5301−5310

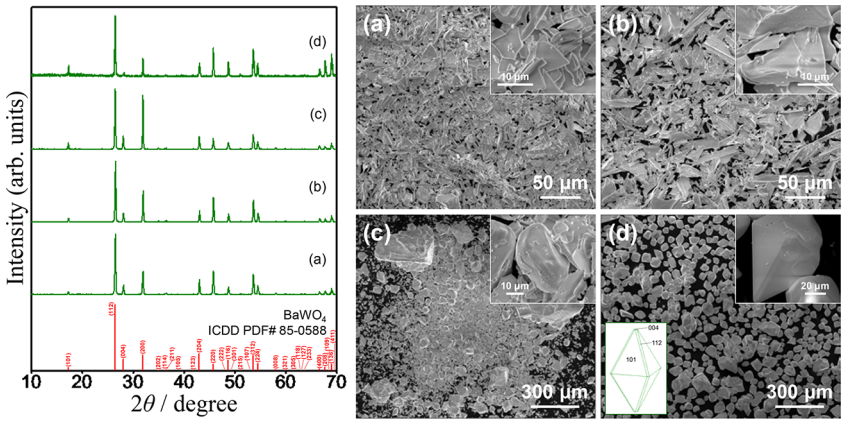

Figure 3. XRD patterns and SEM images of the $BaWO_4$ crystals grown using the NaCl flux with solute concentrations: (a) 5, (b) 10, (c) 20, and (d) 50 mol %.

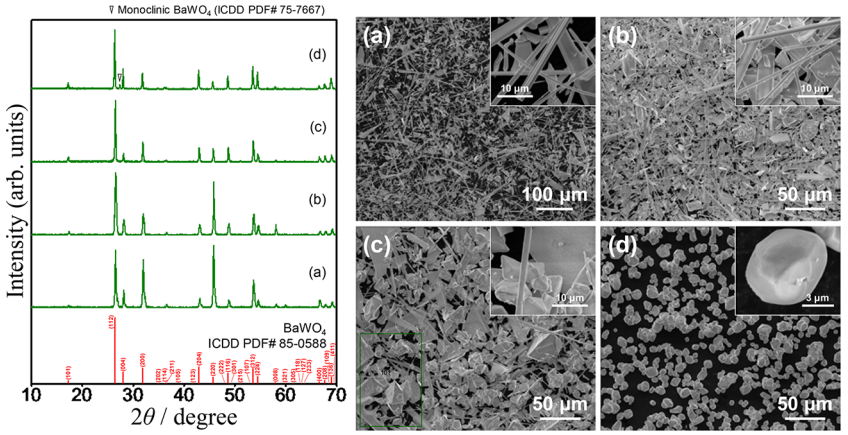

Figure 4. XRD patterns and SEM images of the $BaWO_4$ crystals grown using the KCl flux with solute concentrations: (a) 5, (b) 10, (c) 20, and (d) 50 mol %.

NaCl) and 4.5 mol % (21 g/100 g KCl), respectively, which is in good agreement with the above-mentioned contents. The effect of the flux on the morphology of $SrWO_4$ crystals was confirmed by synthesizing $SrWO_4$ crystals without any fluxes (a solid-state reaction). As shown in Figure S3a, the $SrWO_4$ crystals synthesized via a solid-state reaction possess a spherical shape with smooth surfaces, whereas the chloride flux-grown $SrWO_4$ crystals display unique and idiomorphic shapes as discussed earlier. Chloride fluxes have the potential for designing the morphology of $SrWO_4$ crystals.

Effect of Flux and Solute Concentration on Growth of $BaWO_4$ Crystals. We also studied the crystal-growth condition effect (flux and solute concentration) on the phase formation and morphology of the as-grown $BaWO_4$ crystals. Figure 3 shows the XRD patterns of the crystals grown using the NaCl flux with different solute concentrations (5−50 mol %). All the recorded patterns had diffraction peaks corresponding to tetragonal $BaWO_4$ (ICDD PDF# 85-0588). At a solute concentration of 20 mol %, the (200)/(112) peak intensity ratio of 0.70 was higher than that of the reference (0.24), which is because our $BaWO_4$ crystals contain abundant {100} facets. The SEM images of the $BaWO_4$ crystals grown using the NaCl flux with different solute concentrations are shown in Figure 3. At lower solute concentrations (5 and 10 mol %), the as-grown $BaWO_4$ crystals took the shape of irregular plates. Using a solute concentration of 20 mol %, both relatively small platelets and large granular particles (30−300 μm) were grown. The solutions containing 50 mol % solute gave only a nonuniform crystal shapes but with a relatively consistent size of about 69 μm. The as-grown crystals with well-developed crystal facets had an octadecagonal shape with exposed {112}, {101}, and {001} facets.

The XRD patterns of the crystal products grown using the KCl flux with different solute concentrations (5−50 mol %) are shown in Figure 4. The diffraction peaks of the crystals grown with solute concentrations of 5, 10, and 20 mol % were almost identical to a tetragonal $BaWO_4$ phase without any other secondary or impurity peaks. When the solute concentration was 50 mol %, the formation of $BaWO_4$ with a monoclinic crystal structure (ICDD PDF# 75-7667) was confirmed. At lower concentrations of 5 and 10 mol %, the intensity ratios of the (220) peak to the (112) peak were 1.28 and 0.58, respectively. These values were drastically larger than the corresponding intensity ratio (0.10) of the reference. The crystals grown with a solute concentration of 5 mol % had a peak intensity ratio (200)/(112) of 0.56, which was also much larger compared to the reference value (0.24). These differences suggest that the high-temperature nonaqueous solutions containing less than 10 mol % solute produce crystals containing abundant {110} and/or {100} facets. Figure 4 shows SEM images of the $BaWO_4$ crystals grown using KCl flux with different solute concentrations. With a solute concentration of 5 mol %, the as-grown $BaWO_4$ crystals exhibited whisker- and plate-like morphologies. The $BaWO_4$

DOI: 10.1021/acs.cgd.8b00757
Cryst. Growth Des. 2018, 18, 5301−5310

crystals grown with solute concentrations of 10 and 20 mol % have three types of shapes: whisker, platelet, and octadecagon (10 mol %: ca. 30 μm; 20 mol %: 5−70 μm). Increases in the solute concentration from 10 to 20 mol % resulted in increasing the (octadecagon)/(whisker + platelet) quantity ratio visually. Especially at the solute concentration of 20 mol %, the $BaWO_4$ crystals having well-developed crystal facets became an octadecagon bounded by {112}, {101}, and {001} facets. When the concentration of solute was 50 mol %, the $BaWO_4$ polyhedrons (ca. 10 μm) with rounded edges were grown.

The morphology of the chloride flux-grown $BaWO_4$ crystals was sensitively affected by variation in the solute concentration. The crystal shape transition also varies with solute concentration and solubility (NaCl: platelet/dendrite → octadecagon/polyhedron; KCl: whisker/dendrite → platelet → hexadecagon/octadecagon → polyhedron) and will be discussed in detail later in the paper. Intriguingly, at lower solute concentrations, the dendrite projections were formed from the $BaWO_4$ whiskers and platelets. As is the case in $SrWO_4$, the $BaWO_4$ crystal size was proportional to the solubility of $BaWO_4$ in the flux. In accordance with the reported empirical law,[46] the solubility of a barium tungstate in an alkali metal chloride is in proportion to the size difference between barium and alkali metal ions. Hence, since the difference between the cation sizes of Ba^{2+} (r_{ionic} = 1.42 Å: CN = 8) and Na^+ (r_{ionic} = 1.02 Å: CN = 6) is higher than that of Ba^{2+} and K^+ (r_{ionic} = 1.38 Å: CN = 6), the NaCl solubility should become much higher than the KCl solubility.[47] Previous studies have shown that the solubilities of $BaWO_4$ in NaCl and KCl at 900 °C are 16.2 mol % (127 g/100 g NaCl) and 7.2 mol % (40 g/100 g KCl), respectively.[28,32] Accordingly, there are no contradictions between the empirical law and these experimental results. Solid-state synthesis of $BaWO_4$ was performed to confirm the flux effect on the $BaWO_4$ crystal morphology. As indicated in Figure S3b, the as-synthesized $BaWO_4$ particles did not show clear facets owing to low solubility of the reactants ($BaCO_3$ and WO_3). In contrast, several idiomorphic $BaWO_4$ crystal morphologies were developed by using chloride fluxes. Therefore, chloride fluxes strongly affect the crystal shape deformation of $BaWO_4$.

TEM Studies. To analyze the crystallographic orientation in the chloride flux-grown $SrWO_4$ and $BaWO_4$ crystals, further morphological studies were performed using TEM techniques. The bright-field TEM images and corresponding selected-area electron diffraction (SAED) patterns of the $SrWO_4$ and $BaWO_4$ crystals grown using the chloride fluxes with different solute concentrations are shown in Figures 5−8. The spot-like SAED patterns, which were obtained from parts of all the as-grown crystals (red-circled areas), imply the single crystalline nature of the flux-grown $SrWO_4$ and $BaWO_4$ crystals (Figures 5−8). Additionally, the SAED patterns seen in Figures 5−8 can be indexed to the $SrWO_4$ and $BaWO_4$ phases (space group: $I4_1/a$ with a = 5.417 Å and c = 11.940 Å; space group: $I4_1/a$ with a = 5.614 Å and c = 12.719 Å), respectively.[51,52] As clearly seen in Figures 5a,d and 6a,c, the SAED patterns indicate that the $SrWO_4$ whiskers grow along the [001], [110], and [001] directions. The *in-plane* surfaces of the $SrWO_4$ platelets correspond to the (010) lattice plane (Figures 5b and 6b,d), indicating that the as-grown $SrWO_4$ platelets grow laterally in the {101} direction. The SAED patterns seen in Figure 8a,c,e show that the $BaWO_4$ whiskers grow along the [001] direction. As shown in Figures 7a−c, and 8b,d,f, the in-plane surfaces of the $BaWO_4$ platelets lie on the (110) lattice plane. Accordingly, the $BaWO_4$ platelets were grown laterally along the {110} in plane orientation. It is worthwhile to note that almost all of the AWO_4 platelets (A = Sr, Ba) have thicker parts nestled along the edges of the platelets and the growth directions of these thicker parts are the same as the growth directions of the AWO_4 whiskers (Figures 5b, 6b,d, 7c, and 8b,d). The similarity in growth direction suggest that the AWO_4 platelets should be associated in some way with the AWO_4 whiskers.

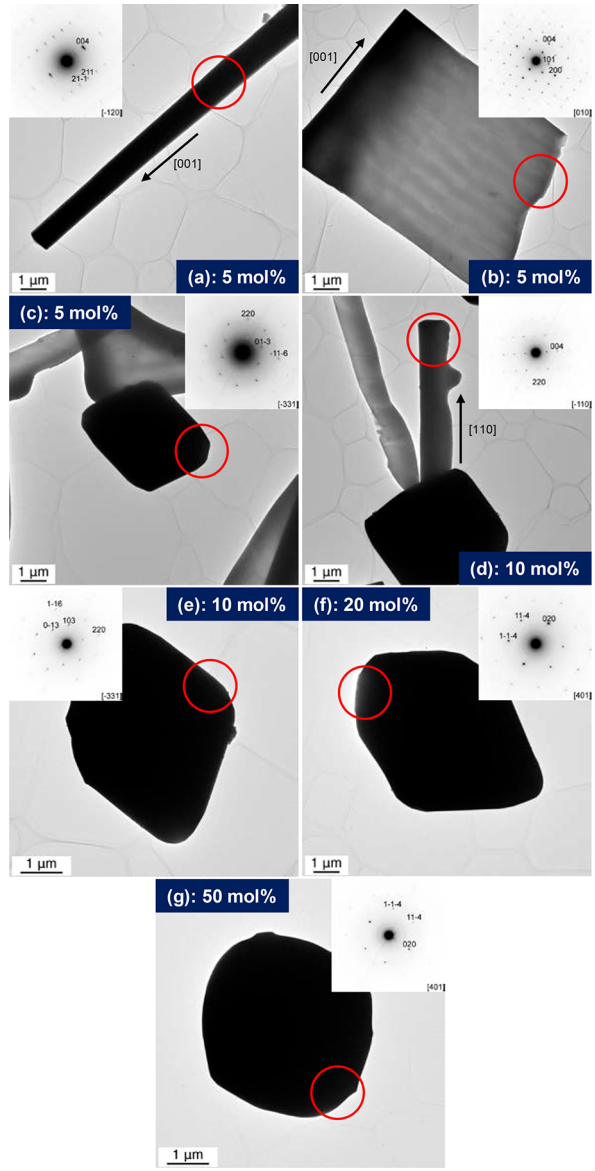

Figure 5. (a−g) Bright-field TEM images and SAED patterns of the $SrWO_4$ crystals grown using the NaCl flux with solute concentrations: 5, 10, 20, and 50 mol %.

Crystal Phase Transition and Morphological Development Mechanism. The mechanism of chloride flux growth for the $SrWO_4$ and $BaWO_4$ crystals with different morphologies was further investigated and discussed in detail. To investigate the phase formation processes of the $SrWO_4$ and $BaWO_4$ crystals, a series of crystal products were grown at different temperatures (300, 600, and 900 °C) for zero holding time by a solid-state reaction. The XRD results shown in Figure S4 reveal that the main $SrWO_4$ and $BaWO_4$ phases were

DOI: 10.1021/acs.cgd.8b00757
Cryst. Growth Des. 2018, 18, 5301−5310

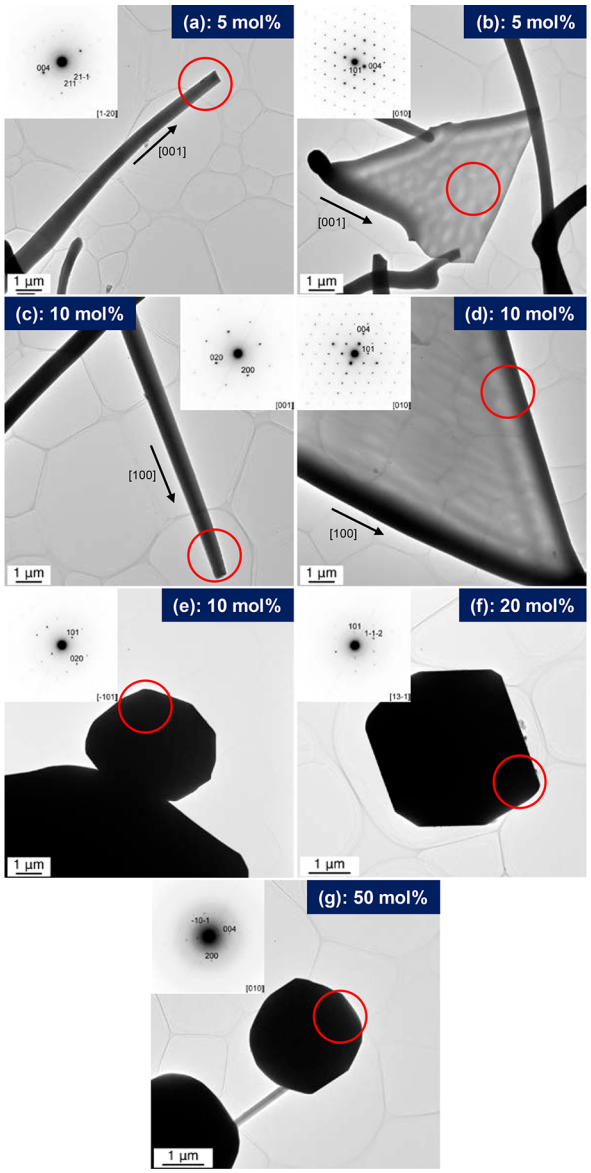

Figure 6. (a–g) Bright-field TEM images and SAED patterns of the $SrWO_4$ crystals grown using the KCl flux with solute concentrations: 5, 10, 20, and 50 mol %.

directly formed from the starting materials upon increasing the temperature to 900 °C.

$$ACO_3 + WO_3 \rightarrow AWO_4 + CO_2 \uparrow (A = \mathrm{Sr},\ \mathrm{Ba})$$

In a flux method, the solute is generally dissolved into the flux partially or completely, and then the crystals are grown from the high-temperature nonaqueous solution due to the lowering of solubility via supercooling or evaporating of the flux at the high temperature as a driving force for crystallization. In order to make a clear distinction about which is the dominant driving force trigger for $SrWO_4$ and $BaWO_4$ crystallization, all the flux evaporation rates were calculated as listed in Table S1. As all the flux evaporation rates were relatively low (<17 wt %), the dominant driving force for crystallization trigger is supercooling in this study.

As we have seen, the flux-grown $SrWO_4$ and $BaWO_4$ crystals have three basic shapes: whisker, platelet, and polyhedron. From the SEM results, when the solute concentration exceeds

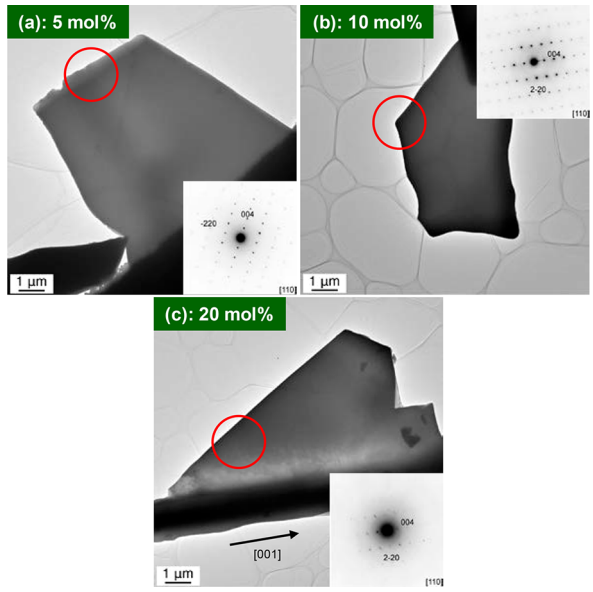

Figure 7. (a–c) Bright-field TEM images and SAED patterns of the $BaWO_4$ crystals grown using the NaCl flux with solute concentrations: 5, 10, and 20 mol %.

the saturated solubility, the $SrWO_4$ and $BaWO_4$ polyhedrons started to nucleate and grow. The quantity of $SrWO_4$ and $BaWO_4$ polyhedrons increases, accordingly as the solute concentration increases. Thus, the $SrWO_4$ and $BaWO_4$ polyhedrons might be produced from the undissolved solute. On the other hand, the $SrWO_4$ and $BaWO_4$ whiskers and platelets might be generated through a dissolution–reprecipitation process. These arguments are in good agreement with a previous study regarding $MgWO_4$, $CaWO_4$, and $BaWO_4$ crystal growth in molten KCl.[33]

The $SrWO_4$ and $BaWO_4$ crystals were grown using a KCl flux with a solute concentration of 5 mol % without removing the flux with water for the purpose of specifying the growth position for each crystal with different shapes in the crucible. The as-obtained crystal products ($SrWO_4$/$BaWO_4$ + KCl) were observed using SEM. The $SrWO_4$ and $BaWO_4$ whiskers and platelets were grown from the inside (and bottom) walls toward the center of the crucible (Figures S5b1,2 and c2,4). As indicated in Figure S5b3,c3, the nucleation sites for the $SrWO_4$ and $BaWO_4$ whiskers were clearly observed. Thereby, the crucible might provide sites for heterogeneous nucleation. Meanwhile, the $SrWO_4$ and $BaWO_4$ polyhedrons precipitated on the crucible bottom (Figure S5b4).

The above results for the chloride flux growth process of the AWO_4 crystals (A = Sr, Ba) were merged into the schematic illustration shown in Figure 9. During the heating process (room temp. → 900 °C), the starting materials are completely converted to AWO_4, and the partial/complete dissolution of the formed AWO_4 crystals into the chloride flux (MCl: M = Na, K) occurs simultaneously. While a high temperature (900 °C) was maintained for 10 h, the crystal surface dissolution and crystallization constantly continued onto the undissolved AWO_4 crystals in the high-temperature nonaqueous solution, in which the undissolved AWO_4 crystals exhibit the lowest energy crystal faces for the conditions and their crystal size is enlarged owing to flux-assisted Ostwald ripening.[48−50] By cooling of the high-temperature solution consisting of a binary mixture of AWO_4 and MCl, the AWO_4 nucleus forming on the

DOI: 10.1021/acs.cgd.8b00757
Cryst. Growth Des. 2018, 18, 5301−5310

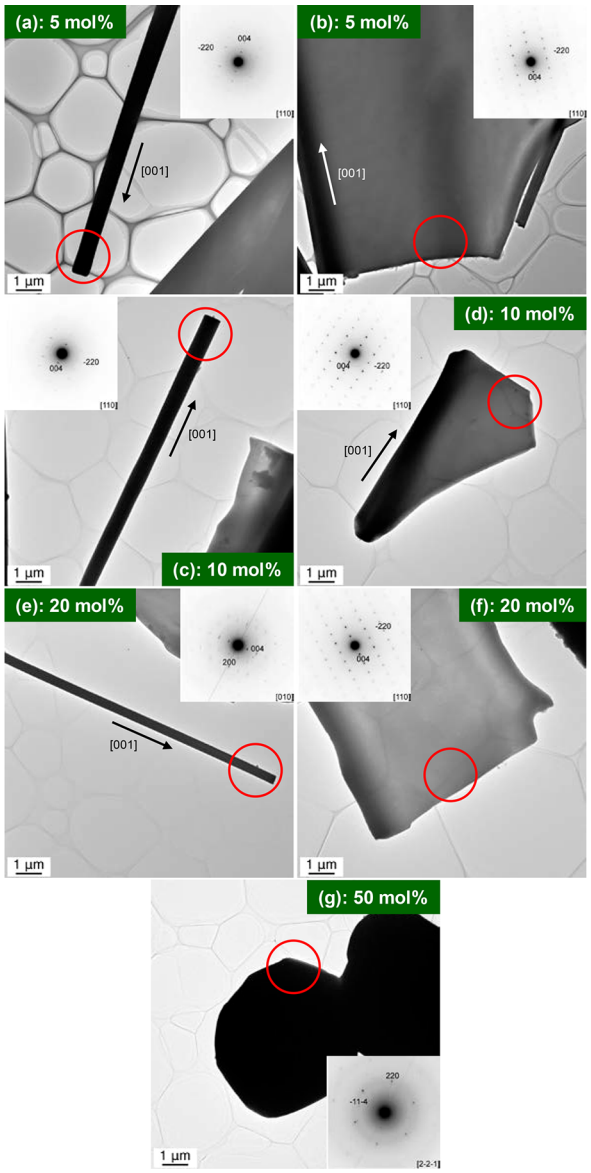

Figure 8. (a–g) Bright-field TEM images and SAED patterns of the $BaWO_4$ crystals grown using the KCl flux with solute concentrations: 5, 10, 20, and 50 mol %.

inner walls of the crucible is caused in conjunction with the crystallization of the dissolved solute onto both the AWO_4 nucleus and the undissolved particles. When the temperature drops below the melting point of the chloride flux (NaCl: 801 °C; KCl: 771 °C),[53] the crystal growth of AWO_4 whiskers and platelets and crystallization of the dissolved solute onto the undissolved particles ceases because of the solidification of the chloride flux.

Further details on the relationship between AWO_4 whiskers and platelets were acquired via SEM and TEM. From the results (Figures 1–8), most of the AWO_4 platelets have thicker parts which are located along the edges or centers of the platelets. Moreover, these line-shaped thicker parts have the same growth directions as the AWO_4 whiskers. On the basis of these findings, we propose the dendritic morphological transformation of the AWO_4 crystal (whisker → dendrite → platelet) during the crystal growth, the process of which can be described as follows (Figure 10a): (i) the AWO_4 whiskers grow from the inner walls of the crucible and fully cover those walls; (ii) the branches grow from one of the two sides of the AWO_4 whiskers; (iii) crystallization of the remaining dissolved solute between the branches occurs at the same time; and (iv) the branches are deformed to plates.[54] Endo et al. and Oishi et al. previously reported the symbiosis of needle, dendrite, and platelet crystals in KCl flux growth of $BaWO_4$ and $CaWO_4$ crystals.[33,55] As shown in Figure 10b,c, the AWO_4 dendrites, which were observed on all the whisker- and platelet-formed conditions, might be intermediates during the morphological transformation. Here, there are two possible factors contributing to the anisotropic growth of the AWO_4 platelets, as given below: (a) the effect of minimizing surface free-energy and (b) a flux-capping effect to form specific crystal facets. According to the surface free-energy effect, the crystals generally tend to grow to exhibit the singular surface having lower surface free-energy on which the constituent atoms are closely and firmly coupled and packed densely. As shown in Figure S6, among the {100}, {010}, {001}, and {110} facets of AWO_4, {001} facets are the densest and have the lowest surface free-energies. Incidentally, the calculated surface free-energies of $SrWO_4$ and $BaWO_4$ are in the sequence {100} = {010} 1.161 $J{\cdot}m^{-2}$ > {110} 0.698 $J{\cdot}m^{-2}$ > {001} 0.527 $J{\cdot}m^{-2}$ and {100} = {010} 0.799 $J{\cdot}m^{-2}$ > {110} 0.445 $J{\cdot}m^{-2}$ > {001} 0.229 $J{\cdot}m^{-2}$, respectively. However, the as-grown $SrWO_4$ and $BaWO_4$ platelets exposed {010} and {110} facets as in-plane surfaces, respectively. Consequently, the anisotropic growth of the

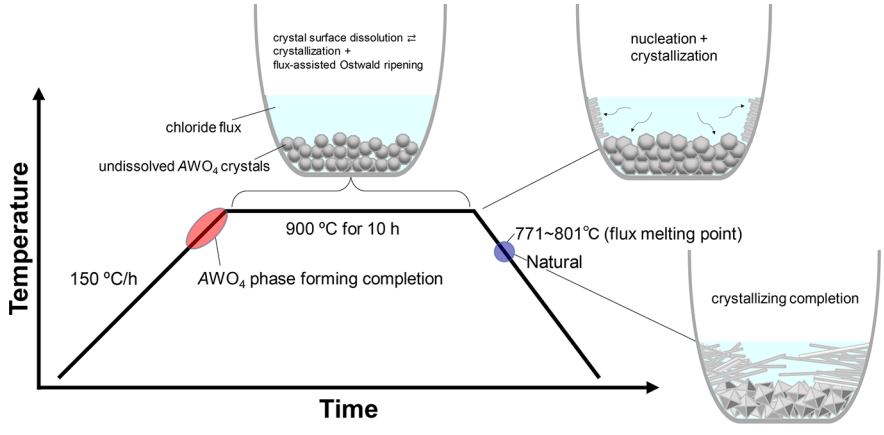

Figure 9. Schematic illustration of the chloride flux growth process of the AWO_4 crystals (A = Sr, Ba).

DOI: 10.1021/acs.cgd.8b00757
Cryst. Growth Des. 2018, 18, 5301–5310

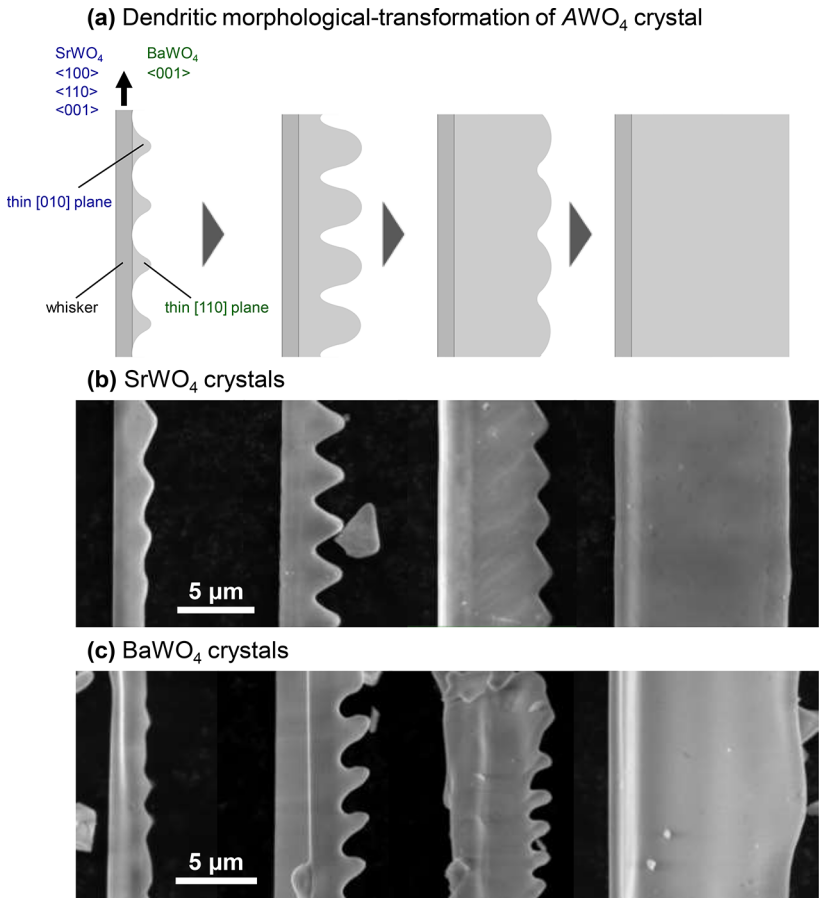

Figure 10. (a) Schematic illustration of proposed morphological transformation mechanism of the chloride flux-grown AWO_4 crystal (whisker → dendrite → platelet). (b and c) SEM images of the typical $SrWO_4$ and $BaWO_4$ whiskers, dendrites, and platelets grown using the NaCl flux with the solute concentration of 5 mol %.

AWO_4 platelets might be caused by chloride flux species acting as a capping agent, which presumably stabilize the $SrWO_4$ (010) and $BaWO_4$ (110) surfaces during the crystal growth and direct the crystallization toward platelet formation.

To understand the solubility and solute concentration impact on the resultant morphology of the flux-grown $SrWO_4$ and $BaWO_4$ crystals, the crystal morphology formation and evolution map for AWO_4 (growth temp.: 900 °C) is presented in Figure S7. Here, the formation and evolution of AWO_4 crystal morphology can be classified into three stages. (1) When the solute concentration is lower than the solubility, AWO_4 whiskers, dendrites, and platelets are formed. In this stage, increasing both the solute concentration and solubility might result in increasing the proportion of AWO_4 platelets because a large amount of dissolved solute allows whiskers to grow into platelets during the crystal growth. (2) Once the solute concentration exceeds the solubility, the faceted AWO_4 polyhedrons are also formed from the undissolved solute. With increasing solute concentration, the proportion of faceted AWO_4 polyhedrons is increased. (3) Further increasing the solute concentration inhibits the formation of AWO_4 whiskers, dendrites, and platelets because at higher solute concentrations a large amount of undissolved solute occupies significant volume near the crucible wall preventing the nucleation and growth of AWO_4 whiskers, dendrites, and platelets. In addition, the less-faceted AWO_4 polyhedrons start to increase in quantity. Consequently, controlling parameters such as solute concentration and solubility enables the crystal shape control of AWO_4 via the flux method.

CONCLUSIONS

In this study, highly crystalline $SrWO_4$ and $BaWO_4$ whiskers, dendrites, platelets, and polyhedrons were successfully grown by a NaCl- and KCl-flux method. The trend in the dominant crystal-shape transition (whisker → platelet → well/less-faceted polyhedron), which is caused by increasing the solute concentration, did not depend on cation species of either solute or flux (i.e., Sr^{2+}, Ba^{2+}, Na^+, and K^+), but the flux cation species (i.e., Na^+ and K^+) contributed to the crystal size. On the other hand, the solute concentration and flux-solubility played quite important roles in morphological formation and evolution of $SrWO_4$ and $BaWO_4$ crystals. Furthermore, we explained details of chloride flux growth mechanism for each $SrWO_4$ and $BaWO_4$ crystal shape. Both the whisker- and plate-like crystals are grown through the dissolution–nucleation–crystallization process, whereas the polyhedral crystals are formed through a crystal surface modification route via crystal surface dissolution and crystallization. Importantly, it was found that the chloride flux might act as a capping agent and induce the dendritic morphological transformation of the AWO_4 crystal (whisker → dendrite → platelet). Our findings and the techniques of this study can be applied to the chloride flux growth of high-quality oxide crystals with unique morphologies, which could be useful for various applications.

DOI: 10.1021/acs.cgd.8b00757
Cryst. Growth Des. 2018, 18, 5301–5310

■ ASSOCIATED CONTENT

Supporting Information

The Supporting Information is available free of charge on the ACS Publications website at DOI: 10.1021/acs.cgd.8b00757.

Schematic illustrations of the crystal structures of $SrWO_4$ and $BaWO_4$; experimental procedure for the measuring the solubility of $SrWO_4$ in KCl flux heated at 900 °C; XRD patterns and SEM images of $SrWO_4$ and $BaWO_4$ crystals grown by using a solid-state reaction (holding temp.: 300, 600, and 900 °C; holding time: 0 and 10 h); flux evaporation rates; digital photographs and SEM images of the crystal products (AWO_4 + KCl: A = Sr, Ba); Schematic illustrations of crystal facets on AWO_4 (A = Sr, Ba); Map of the crystal morphology formation and evolution for AWO_4 (A = Sr, Ba) (PDF)

■ AUTHOR INFORMATION

Corresponding Author

*E-mail: mullins@che.utexas.edu.

ORCID

Kenta Kawashima: 0000-0001-7318-6115
Yang Liu: 0000-0002-7240-1546
Jie Lin: 0000-0002-1281-9713
Graeme Henkelman: 0000-0002-0336-7153
C. Buddie Mullins: 0000-0003-1030-4801

Author Contributions

◆K.K. and J.H.K. contributed equally.

Notes

The authors declare no competing financial interest.

■ ACKNOWLEDGMENTS

The authors gratefully acknowledge the U.S. Department of Energy Basic Energy Sciences Grant DE-FG02-09ER16119 (C.B.M.) for support of the experimental portion of the paper and DE-SC0010576 (G.H.) for the computational portion of the study. We also acknowledge the Welch Foundation for their generous support through grants F-1436 (C.B.M) and F-1841 (G.H.).

■ REFERENCES

(1) Yoon, S. H.; Kim, D. W.; Cho, S. Y.; Hong, K. S. Investigation of the relations between structure and microwave dielectric properties of divalent metal tungstate compounds. *J. Eur. Ceram. Soc.* **2006**, *26*, 2051−2054.

(2) Modi, D.; Srinivas, M.; Tawde, D.; Murthy, K. V. R.; Verma, V.; Patel, N. Hydrothermal synthesis and photoluminescence properties of cerium-doped cadmium tungstate nanophosphor. *J. Exp. Nanosci.* **2015**, *10*, 777−786.

(3) Vidya, S.; Solomon, S.; Thomas, J. K. Synthesis, characterization, and low temperature sintering of nanostructured $BaWO_4$ for optical and LTCC applications. *Adv. Condens. Matter Phys.* **2013**, *2013*, 409620.

(4) Korzhik, M.; Lecoq, P. Search of new scintillation materials for nuclear medicine applications. *IEEE Trans. Nucl. Sci.* **2001**, *48*, 628−631.

(5) Li, C.; Liang, Y.; Mao, J.; Ling, L.; Cui, Z.; Yang, X.; Zhu, S.; Li, Z. Enhancement of gas-sensing abilities in p-type $ZnWO_4$ by local modification of Pt nanoparticles. *Anal. Chim. Acta* **2016**, *927*, 107−116.

(6) Chen, D.; Liu, Z.; Ouyang, S.; Ye, J. Simple room-temperature mineralization method to $SrWO_4$ micro/nanostructures and their photocatalytic properties. *J. Phys. Chem. C* **2011**, *115*, 15778−15784.

(7) Sahmi, A.; Bensadok, K.; Zirour, H.; Trari, M. Physical and photoelectrochemical characterizations of $SrWO_4$ prepared by thermal decomposition. Application to the photo electro-oxidation of ibuprofen. *J. Solid State Electrochem.* **2017**, *21*, 2817−2824.

(8) Itoh, M.; Fujita, M. Optical properties of scheelite and raspite $PbWO_4$ crystals. *Phys. Rev. B: Condens. Matter Mater. Phys.* **2000**, *62*, 12825.

(9) Maurera, M. A. M. A.; Souza, A. G.; Soledade, L. E. B.; Pontes, F. M.; Longo, E.; Leite, E. R.; Varela, J. A. Microstructural and optical characterization of $CaWO_4$ and $SrWO_4$ thin films prepared by a chemical solution method. *Mater. Lett.* **2004**, *58*, 727−732.

(10) Shan, Z.; Wang, Y.; Ding, H.; Huang, F. Structure-dependent photocatalytic activities of MWO_4 (M = Ca, Sr, Ba). *J. Mol. Catal. A: Chem.* **2009**, *302*, 54−58.

(11) Momma, K.; Izumi, F. VESTA 3 for three-dimensional visualization of crystal, volumetric and morphology data. *J. Appl. Crystallogr.* **2011**, *44*, 1272−1276.

(12) Cheng, L.; Liu, P.; Qu, S. X.; Zhang, H. W. Microwave dielectric properties of AWO_4 (A = Ca, Ba, Sr) ceramics synthesized via high energy ball milling method. *J. Alloys Compd.* **2013**, *581*, 553−557.

(13) Sczancoski, J. C.; Avansi, W.; Costa, M. G. S.; Li, M. S.; Mastelaro, V. R.; Santos, R. S.; Longo, E.; Cavalcante, L. S. Effect of different strontium precursors on the growth process and optical properties of $SrWO_4$ microcrystals. *J. Mater. Sci.* **2015**, *50*, 8089−8103.

(14) Lou, Z.; Cocivera, M. Cathodoluminescence of $CaWO_4$ and $SrWO_4$ thin films prepared by spray pyrolysis. *Mater. Res. Bull.* **2002**, *37*, 1573−1582.

(15) Li, X.; Song, Z.; Qu, B. Shape-controlled electrochemical synthesis of $SrWO_4$ crystallites and their optical properties. *Ceram. Int.* **2014**, *40*, 1205−1208.

(16) Hasegawa, S. Crystal growth by flux method. *Kobutsugaku Zasshi* **1968**, *8*, 397−406 (in Japanese).

(17) Teshima, K.; Hara, Y.; Yubuta, K.; Oishi, S.; Domen, K.; Hojamberdiev, M. Application of flux method to the fabrication of $Ba_5Ta_4O_{15}$, $Sr_5Ta_4O_{15}$, $Sr_2Ta_2O_7$, and $BaTaO_2N$ polycrystalline films on Ta substrates. *Cryst. Growth Des.* **2017**, *17*, 1583−1588.

(18) Bugaris, D. E.; zur Loye, H. C. Materials discovery by flux crystal growth: quaternary and higher order oxides. *Angew. Chem. Int. Ed.* **2012**, *51*, 3780−3811.

(19) Yamada, T.; Sukegawa, Y.; Wagata, H.; Yubuta, K.; Teshima, K. Facile growth of centimeter-order, highly crystalline $ZnWO_4$ single crystals by the flux evaporation technique using molten NaCl. *CrystEngComm* **2016**, *18*, 8608−8613.

(20) Yamada, T.; Murata, Y.; Wagata, H.; Yubuta, K.; Teshima, K. Facile morphological modification of $Ba_5Nb_4O_{15}$ crystals using chloride flux and in situ growth investigation. *Cryst. Growth Des.* **2016**, *16*, 3954−3960.

(21) Sudare, T.; Kawaura, D.; Yubuta, K.; Hayashi, F.; Teshima, K. Growth of {100}-faceted $NaFeTiO_4$ crystals with a tunable aspect ratio from a NaCl−Na_2SO_4 binary flux. *CrystEngComm* **2018**, *20*, 873−878.

(22) Lv, X. S.; Sun, Y. L.; Han, J.; Gu, G. X.; Wan, S. M.; Cheng, M. J.; Pan, S. L.; Zhang, Q. L. Growth and Raman spectrum of $Ba_2Mg(B_3O_6)_2$ crystal. *J. Cryst. Growth* **2013**, *363*, 220−225.

(23) Kestigian, M. Yttrium-iron garnet single-crystal growth by the combined Czochralski-molten salt solvent technique. *J. Am. Ceram. Soc.* **1967**, *50*, 165−166.

(24) Oishi, S.; Yamamoto, H. Growth of emerald crystals by evaporation of a K_2O−MoO_3 flux. *J. Mater. Chem.* **1996**, *6*, 1687−1691.

(25) Oishi, S.; Tate, I.; Hirano, S.; Naka, S. Choice of fluxes for the crystal growth of oxides from high-temperature solutions. *Nippon Kagaku Kaishi* **1984**, *5*, 685−690 (in Japanese).

(26) Van Uitert, L. G.; Soden, R. R. Single crystal tungstates for resonance and emission studies. *J. Appl. Phys.* **1960**, *31*, 328−330.

(27) Brixner, L. H.; Babcock, K. Inorganic single crystals from reactions in fused salts. *Mater. Res. Bull.* **1968**, *3*, 817−824.

DOI: 10.1021/acs.cgd.8b00757
Cryst. Growth Des. 2018, 18, 5301−5310

(28) Voigt, D. O.; Neels, H. Wachstumsformen von tetragonalen erdalkaliwolframaten in schmelzlösungen und deren deutung. *Krist. Tech.* **1971**, *6*, 651−658 (in German).
(29) Packter, A.; Roy, B. N. The kinetics of crystallisation of alkaline-earth metal tungstates from solution in lithium chloride melts. *J. Cryst. Growth* **1973**, *18*, 86−93.
(30) Patel, A. R.; Arora, S. K. Growth of single crystals of barium tungstate by double decomposition in melt. *J. Cryst. Growth* **1973**, *18*, 175−178.
(31) Patel, A. R.; Arora, S. K. Crystal growth of $BaWO_4$ and $SrWO_4$ by flux evaporation. *J. Cryst. Growth* **1974**, *23*, 95−100.
(32) Oishi, S.; Kobayashi, T.; Tate, I.; Endo, Y. Growth of $BaWO_4$ needle crystals by KCl flux method. *Nippon Kagaku Kaishi* **1978**, *9*, 1228−1231 (in Japanese).
(33) Endo, Y.; Oishi, S.; Kanazawa, Y.; Tate, I. Growth and morphology of some alkaline-earth metal tungstate crystals from KCl flux. *Bull. Geol. Surv. Japan* **1986**, *37*, 53−66 (in Japanese).
(34) Romanyuk, Y. E.; Ehrentraut, D.; Pollnau, M.; García-Revilla, S.; Valiente, R. Low-temperature flux growth of sulfates, molybdates, and tungstates of Ca, Sr, and Ba and investigation of doping with Mn^{6+}. *Appl. Phys. A: Mater. Sci. Process.* **2004**, *79*, 613−618.
(35) Arora, S. K.; Chudasama, B. Crystallization and optical properties of $CaWO_4$ and $SrWO_4$. *Cryst. Res. Technol.* **2006**, *41*, 1089−1095.
(36) Jiang, X.; Ma, J.; Yao, Y.; Sun, Y.; Liu, Z.; Ren, Y.; Liu, J.; Lin, B. Low-temperature synthesis of $SrWO_4$ nano-particles by a molten salt method. *Ceram. Int.* **2009**, *35*, 3525−3528.
(37) Sun, X.; Sun, X.; Li, X.; He, J.; Wang, B. Molten salt synthesis, characterization, and luminescence of $SrWO_4$, $SrWO_4$:Tb^{3+} and $SrWO_4$:Eu^{3+} powders. *J. Mater. Sci.: Mater. Electron.* **2014**, *25*, 2320−2324.
(38) Pinho, S. P.; Macedo, E. A. Solubility of NaCl, NaBr, and KCl in water, methanol, ethanol, and their mixed solvents. *J. Chem. Eng. Data* **2005**, *50*, 29−32.
(39) Oishi, S.; Sugiura, I. Growth of chlorapatite crystals from a sodium chloride flux. *Bull. Chem. Soc. Jpn.* **1997**, *70*, 2483−2487.
(40) Kresse, G.; Hafner, J. Ab initio molecular dynamics for liquid metals. *Phys. Rev. B: Condens. Matter Mater. Phys.* **1993**, *47*, 558−561.
(41) Kresse, G.; Furthmüller, J. Efficiency of ab-initio total energy calculations for metals and semiconductors using a plane-wave basis set. *Comput. Mater. Sci.* **1996**, *6*, 15−50.
(42) Kresse, G.; Furthmüller, J. Efficient iterative schemes for ab initio total-energy calculations using a plane-wave basis set. *Phys. Rev. B: Condens. Matter Mater. Phys.* **1996**, *54*, 11169−11186.
(43) Blöchl, P. E. Projector augmented-wave method. *Phys. Rev. B: Condens. Matter Mater. Phys.* **1994**, *50*, 17953−17979.
(44) Perdew, J. P.; Burke, K.; Ernzerhof, M. Generalized gradient approximation made simple. *Phys. Rev. Lett.* **1996**, *77*, 3865−3868.
(45) Hammer, B. H. L. B.; Hansen, L. B.; Nørskov, J. K. Improved adsorption energetics within density-functional theory using revised Perdew-Burke-Ernzerhof functionals. *Phys. Rev. B: Condens. Matter Mater. Phys.* **1999**, *59*, 7413−7421.
(46) Roy, B. N. Thermodynamic analysis of solute-solvent interactions in the solubility-temperature relations of alkaline-earth metal tungstates and sodium tungstate. *Cryst. Res. Technol.* **1983**, *18*, 269−273.
(47) Shannon, R. D. Revised effective ionic radii and systematic studies of interatomic distances in halides and chalcogenides. *Acta Crystallogr., Sect. A: Cryst. Phys., Diffr., Theor. Gen. Crystallogr.* **1976**, *32*, 751−767.
(48) Bowker, M. Surface science: The going rate for catalysts. *Nat. Mater.* **2002**, *1*, 205−206.
(49) Hojamberdiev, M.; Kawashima, K.; Kumar, M.; Yamakata, A.; Yubuta, K.; Gurlo, A.; Hasegawa, M.; Domen, D.; Teshima, K. Engaging the flux-grown $La_{1-x}Sr_xFe_{1-y}Ti_yO_3$ crystals in visible-light-driven photocatalytic hydrogen generation. *Int. J. Hydrogen Energy* **2017**, *42*, 27024−27033.
(50) Kawashima, K.; Hojamberdiev, M.; Yubuta, K.; Domen, K.; Teshima, K. Synthesis and visible-light-induced sacrificial photocatalytic water oxidation of quinary oxynitride $BaNb_{0.5}Ta_{0.5}O_2N$ crystals. *J. Energy Chem.* **2017**, DOI: 10.1016/j.jechem.2017.09.006.
(51) Pereira, P. F. S.; de Moura, A. P.; Nogueira, I. C.; Lima, M. V. S.; Longo, E.; de Sousa Filho, P. C.; Nassar, E. J.; Rosa, I. L. V.; Serra, O. A. Study of the annealing temperature effect on the structural and luminescent properties of $SrWO_4$: Eu phosphors prepared by a non-hydrolytic sol−gel process. *J. Alloys Compd.* **2012**, *526*, 11−21.
(52) Gürmen, E.; Daniels, E.; King, J. S. Crystal structure refinement of $SrMoO_4$, $SrWO_4$, $CaMoO_4$, and $BaWO_4$ by neutron diffraction. *J. Chem. Phys.* **1971**, *55*, 1093−1097.
(53) Kawashima, K.; Hojamberdiev, M.; Mabayoje, O.; Wygant, B. R.; Yubuta, K.; Mullins, C. B.; Domen, K.; Teshima, K. NH_3-assisted chloride flux-coating method for direct fabrication of visible-light-responsive $SrNbO_2N$ crystal layers. *CrystEngComm* **2017**, *19*, 5532−5541.
(54) Glicksman, M. E.; Lupulescu, A. O. Dendritic crystal growth in pure materials. *J. Cryst. Growth* **2004**, *264*, 541−549.
(55) Oishi, S.; Endo, Y.; Kobayashi, T.; Tate, I. The effects of M(M = Mg, Ca and Ba) ions on the KCl flux growth of MWO_4 Needle Crystals. *Nippon Kagaku Kaishi* **1979**, *9*, 1191−1197 (in Japanese).

DOI: 10.1021/acs.cgd.8b00757
Cryst. Growth Des. 2018, 18, 5301−5310